A Measure of Multivariate Phase Synchrony Using Hyperdimensional Geometry

Mahmood Al-Khassaweneh, *Senior Member, IEEE*, Marisel Villafañe-Delgado, *Student Member, IEEE*, Ali Yener Mutlu, *Member, IEEE*, and Selin Aviyente, *Member, IEEE*

***Abstract*—Phase synchrony has been used to investigate the dynamics of subsystems that make up a complex system. Current measures of phase synchrony are mostly bivariate focusing on the synchrony between pairs of time series. Bivariate measures do not necessarily lead to a complete picture of the global interactions within a complex system. Current multivariate synchrony measures are based on either averaging all possible pairwise synchrony values or eigendecomposition of the pairwise bivariate synchrony matrix. These approaches are sensitive to the accuracy of the bivariate synchrony indices, computationally complex and indirect ways of quantifying the multivariate synchrony. Recently, we had proposed a method to compute the multivariate phase synchrony using a hyperdimensional coordinate system. This method, referred to as Hyperspherical Phase Synchrony (HPS), has been found to be dependent on the ordering of the phase differences. In this paper, we propose a more general hyperspherical coordinate system along with a new higher-dimensional manifold representation to eliminate the dependency on the ordering of the signals' phases. This new framework, referred to as Hyper-Torus Synchrony (HTS), is shown to be equivalent to the root-mean-square of a sufficient set of squared phase-locking values whose phase differences contain information about all oscillators in the network. The statistical properties of HTS are given analytically and its performance is evaluated thoroughly for both synthetic and real signals.**

***Index Terms*—Multivariate phase synchrony, time-frequency analysis, Rihaczek distribution, electroencephalogram, functional brain connectivity.**

I. Introduction

COORDINATED time-varying interactions are fundamental in dynamical systems, ranging from a few coupled elements to complex networks. Examples of systems of coupled oscillators occur widely in nature and engineering such as circadian rhythms [1], neuroscience [2], flashing fireflies [3], coupled Josephson junctions [4], the Millenium Bridge [5], and others [6]–[9]. In the stochastic sense, synchronization has been defined as an adjustment of rhythms of oscillating objects due to their weak interaction [10] and this adjustment can be described in terms of phase locking and frequency entrainment. Phase locking or phase synchrony between two oscillators occurs when the generalized phase difference, $\Phi_{i,j}(t,\omega) = |\Phi_i(t,\omega) - \Phi_j(t,\omega)| \bmod 2\pi < \text{constant}$, at time t and frequency ω [11], [12]. Two steps are needed for quantifying phase synchrony. First, instantaneous phase of each signal is estimated at a particular frequency of interest through methods such as the Hilbert transform, complex wavelet transform [13], empirical mode decomposition [14]–[18] or the recently proposed Reduced Interference Distribution-Rihaczek (RID-Rihaczek) complex time-frequency distribution [19], [20]. In the second step, the amount of synchrony is quantified through either the entropy of the distribution of the phase differences or mean phase coherence, also known as phase locking value (PLV), which computes the circular variance of the relative phase [21], [22]. Although bivariate PLV has been widely used, it has various disadvantages for the study of large and complex networks. First, PLV does not provide information about the common integrating structure among the ensemble of oscillators. Second, for large data sets multiple computations of pairwise PLV increase computational costs.

Recently, phase synchronization of a group of oscillators, which is referred to as global or multivariate phase synchronization, has been of interest for understanding the group dynamics and characteristic behavior of complex networks [17], [23]–[26]. Contrary to the bivariate phase synchrony, multivariate synchrony captures the global synchronization patterns quantifying the degree of interactions within a group of oscillators. In addition, multivariate synchrony methods provide a single number, rather than a matrix of pairwise synchrony values. One of the earliest approaches to multivariate synchrony analysis was global field synchronization (GFS) proposed by Koenig *et al.* [24]. GFS first transforms the time series data to the frequency domain, and then quantifies the scatter of the multivariate data through the eigenvalues of the covariance matrix between the sine and cosine coefficients of the Fourier transform. This measure inherently assumes the stationarity of the data and cannot capture time-varying aspects of synchrony. Moreover, this method quantifies synchrony as the instance when the phases of the two signals are exactly the same and does not take into account the case of constant phase difference. Knyazeva *et al.* [27] proposed another simple

Manuscript received July 30, 2015; revised December 10, 2015 and January 20, 2016; accepted January 24, 2016. Date of publication February 11, 2016; date of current version April 18, 2016. The associate editor coordinating the review of this manuscript and approving it for publication was Morten Mørup. This work was in part supported by the National Science Foundation under Grants No. CCF-1218377 and DGE-1424871.

M. Al-Khassaweneh is with the Department of Electrical and Computer Engineering, Michigan State University, East Lansing, MI 48824 USA, on leave from Yarmouk University, Irbid, 21163, Jordan (e-mail: alkhass1@msu.edu).

M. Villafañe-Delgado and S. Aviyente are with the Department of Electrical and Computer Engineering, Michigan State University, East Lansing, MI 48824 USA (e-mail: aviyente@egr.msu.edu).

A. Yener Mutlu is with the Department of Computer Engineering, Izmir University of Economics, Izmir 35330, Turkey (e-mail: ali.mutlu@ieu.edu.tr).

Color versions of one or more of the figures in this paper are available online at http://ieeexplore.ieee.org.

Digital Object Identifier 10.1109/TSP.2016.2529586

measure, the multivariate phase synchrony (MPS), defined as the mean phase synchrony averaged across the observation samples. Rudrauf *et al.* [28], on the other hand, proposed an alternative approach to quantifying phase synchrony through frequency locking by exploiting the relationship between phase and frequency and identifying continuous periods of identical instantaneous frequency. Similarly, in [17] the idea of cointegration is used to define multivariate phase synchrony. However, this method can only identify phase synchrony in a nonstatistical sense and is not reliable in the case of noisy signals.

More recently, methods inspired by random matrix theory (RMT) and spectral graph theory were proposed. These methods first compute the bivariate synchrony and then perform cluster analysis through eigendecomposition of the bivariate synchrony matrix as proposed by Allefeld *et al.* [29]. Initial work in this area focused on perceiving the oscillators as constituting a single cluster to which they participate in different degrees [30]. The existence of a single synchronization cluster is not a reasonable assumption since most complex networks usually consist of multiple clusters. In order to address this limitation, approaches based on the eigenvalue decomposition of the pairwise bivariate synchronization matrix have been proposed [31], [32]. However, it has recently been shown in cases where there are clusters of similar strength that are slightly synchronized with each other, the assumed one-to-one correspondence between eigenvectors and clusters is not realistic [33].

In order to capture the connectivity structure with a single number, Saito *et al.* [34] quantified global synchrony through the entropy of the eigenspectrum of the covariance or bivariate connectivity matrix. This measure was then generalized by Stam *et al.* [35] and others as the S-measure [23], [36], [37]. This measure uses the principle of time-delay embedding and indicates how strongly channel k at a given time is synchronized to all other channels. Similar to other methods in nonlinear dynamics, it requires the selection of different parameters, such as a threshold and the time-lag, and is computationally expensive.

Recently, hyperspherical phase synchrony (HPS) was introduced as an alternative method to directly measure the multivariate phase synchronization among a group of oscillators [38], [39]. HPS generalizes bivariate synchrony, where the phase difference between two time series is mapped onto a unit circle, by mapping the $N-1$ phase differences between consecutive oscillators onto an N-dimensional space parameterized by hypespherical coordinates [38]. HPS is advantageous over the S-estimator thanks to its reduced computational complexity and robustness to noise [39]. However, as we show in Section III, we found that this estimator was highly dependent on the ordering of the phase differences parameterizing the hypersphere.

In this paper, we propose a novel measure to estimate the multivariate phase synchrony in a hyperdimensional coordinate system and address the shortcomings of HPS. Two complementary approaches are developed to quantify the circular variance of phase differences among multiple oscillators in a high dimensional space. In the first approach, we extend the hyperspherical coordinate system used in HPS to include redundancies, i.e., x and y coordinates of circles with varying radii, such that the ordering of the phases is not important. In the second approach, we propose a new mapping of the phase differences to a high-dimensional flat torus and compute the magnitude of the mean phase vector in this new geometry resulting in the hyper-torus phase synchrony (HTS). We then show the equivalence of these two metrics, provide analytical bounds on the bias and variance of HTS and show bias correction for HTS squared. We compared the performance of HTS and the S-estimator on simulated networks of chaotic oscillators for sensitivity to coupling strength and network structure. Finally, we consider an application of HTS for quantifying global synchrony in the brain from multichannel electroencephalogram (EEG) signals and compare it to S-estimator.

II. Background

A. Reduced Interference Rihaczek Distribution (RID-Rihaczek)

As mentioned in the Introduction, the computation of phase synchrony relies on an estimate of instantaneous phase. In this work, we will compute the signal's instantaneous phase based on the RID-Rihaczek time-frequency distribution as proposed in [19]. For a signal x_i, define $C_i(t,\omega)$ to be its complex RID-Rihaczek time-frequency distribution, given by

$$C_i(t,\omega) = \int\int \underbrace{\exp\left(-\frac{(\theta\tau)^2}{\sigma}\right)}_{\text{Choi-Williams}} \times \underbrace{\exp\left(j\frac{\theta\tau}{2}\right)}_{\text{Rihaczek}} A_i(\theta,\tau) e^{-j(\theta t+\tau\omega)} d\tau d\theta, \quad (1)$$

where $A_i(\theta,\tau)$ is the ambiguity function of x_i:

$$A_i(\theta,\tau) = \int x_i\left(u+\frac{\tau}{2}\right) x_i^*\left(u-\frac{\tau}{2}\right) e^{j\theta u} du. \quad (2)$$

The time-varying phase of the signal x_i is computed as

$$\Phi_i(t,\omega) = \arg\left[\frac{C_i(t,\omega)}{|C_i(t,\omega)|}\right]. \quad (3)$$

The phase difference between two signals x_1 and x_2 can be computed as

$$\Phi_{1,2}(t,\omega) = \arg\left[\frac{C_1(t,\omega)}{|C_1(t,\omega)|}\frac{C_2^*(t,\omega)}{|C_2(t,\omega)|}\right]. \quad (4)$$

B. Phase Locking Value

PLV between two signals x_1 and x_2 as a function of time and frequency [40] is defined by

$$\begin{aligned}\mathrm{PLV}_{1,2}(t,\omega) &= \frac{1}{N}\left|\sum_{k=1}^{N}\exp\left(j\Phi_{1,2}^k(t,\omega)\right)\right| \\ &= \sqrt{\left\langle\cos\Phi_{1,2}^k(t,\omega)\right\rangle^2+\left\langle\sin\Phi_{1,2}^k(t,\omega)\right\rangle^2}, \quad (5)\end{aligned}$$

where N corresponds to the total number of trials or realizations of the signal, $\Phi_{1,2}^k(t,\omega)$ is the phase difference between x_1 and

x_2 as defined by (4) for the kth trial and $\langle\cdot\rangle$ denotes averaging over trials. For each trial k, the phase difference $\Phi^k_{1,2}(t,\omega)$ defines a vector on the unit circle. Thus, PLV evaluates the circular variance of the unit vectors across trials. Therefore, PLV approaches 1 if the phase differences over trials exhibit small variation and approaches 0 if there is no synchrony over trials.

C. S-Estimator

The S-estimator at time t and frequency ω is computed as

$$S(t,\omega) = 1 + \frac{\left(\sum_{m=1}^{M} \lambda_m \log(\lambda_m)\right)}{\log(M)}, \tag{6}$$

where $\lambda_m,\ m = 1,\ldots,M$ are the eigenvalues of the bivariate synchronization matrix $\{\mathrm{PLV}_{i,j}(t,\omega)\}, i,j = 1,\ldots,M$, and M is the total number of oscillators in the network [35], [37]. S-estimator is equivalent to 1 minus the entropy of the normalized eigenvalues of the PLV matrix. This measure equals to 1 when all the oscillators are pairwise highly synchronized. In that case, all the entries in the PLV matrix will be equal to one and thus only one eigenvalue will be equal to one. On the other hand, when all the oscillators in the network are not pairwise synchronized the PLV matrix is full rank and its eigenvalues are uniformly distributed, maximizing the entropy and resulting in zero multivariate synchrony.

III. Hyperspherical Phase Synchrony

Bivariate phase synchrony is based on the circular variance of the two-dimensional direction vectors on a unit circle (1-sphere), obtained by mapping the phase differences $\left\{\Phi^k_{1,2}(t,\omega)\right\}_{k=1,\ldots,N}$, where N is the total number of trials, between the two time-series onto a Cartesian coordinate system. If the circular variance of these direction vectors is low, the time-series are said to be locked to each other.

Hyperspherical Phase Synchrony proposed in [38] is an extension of this idea to the multivariate case. Define $\left\{\theta^k_1(t,\omega), \theta^k_2(t,\omega), \ldots, \theta^k_{M-1}(t,\omega)\right\}$ as the $(M-1)$ angular coordinates at time t and frequency ω for the kth trial, where $\theta^k_i(t,\omega) = \Phi^k_i(t,\omega) - \Phi^k_{i+1}(t,\omega)$ is the phase difference between the ith and $(i+1)$th time series within a group of M oscillators. These $(M-1)$ angular coordinates are mapped onto an M-dimensional space by forming direction vectors in an M-dimensional hyperspherical coordinate system. For any natural number M, an $(M-1)$-sphere of radius r is defined as the set of points in (M)-dimensional Euclidean space which are at distance r from a central point, where the radius r may be any positive real number. The set of coordinates in an M-dimensional space, $\gamma_1, \gamma_2, \ldots, \gamma_M$, that define an $(M-1)$-sphere is represented by

$$r^2 = \sum_{i=1}^{M} (\gamma_i - c_i)^2, \tag{7}$$

where $\mathbf{c} = [c_1,\ldots,c_M]$ is the center point and r is the radius. In [38], $r = 1$ and the center point is the origin.

Using the $(M-1)$ angular coordinates, a direction vector $\Gamma^k(t,\omega) = \left[\gamma^k_1(t,\omega),\ldots,\gamma^k_M(t,\omega)\right]$ can be formed by mapping the angular coordinates $(\theta_1,\ldots,\theta_{M-1})$ on a unit $(M-1)$-sphere as[1]:

$$\begin{aligned}
&\gamma^k_1(t,\omega) = \cos\left(\theta^k_1(t,\omega)\right),\\
&\gamma^k_2(t,\omega) = \sin\left(\theta^k_1(t,\omega)\right) \times \cos\left(\theta^k_2(t,\omega)\right),\\
&\gamma^k_3(t,\omega) = \sin\left(\theta^k_1(t,\omega)\right) \times \sin\left(\theta^k_2(t,\omega)\right) \times \cos\left(\theta^k_3(t,\omega)\right),\\
&\qquad\vdots\\
&\gamma^k_{M-1}(t,\omega) = \sin\left(\theta^k_1(t,\omega)\right) \times \cdots \times \sin\left(\theta^k_{M-2}(t,\omega)\right)\\
&\quad\times \cos\left(\theta^k_{M-1}(t,\omega)\right),\\
&\text{and } \gamma^k_M(t,\omega) = \sin\left(\theta^k_1(t,\omega)\right) \times \cdots \times \sin\left(\theta^k_{M-2}(t,\omega)\right)\\
&\quad\times \sin\left(\theta^k_{M-1}(t,\omega)\right).
\end{aligned} \tag{8}$$

Based on this mapping we define the hyperspherical phase synchrony (HPS) as

$$\mathrm{HPS}(t,\omega) = \frac{1}{N}\left|\left|\sum_{k=1}^{N} \Gamma^k(t,\omega)\right|\right|_2, \tag{9}$$

where $\mathrm{HPS}(t,\omega)$ is the multivariate synchronization value at time t and frequency ω, $\|\cdot\|_2$ is the Euclidean norm and N is the number of trials. In the case of perfect multivariate phase synchronization of the network, HPS is equal to 1 and it equals 0 when the oscillators are independent. Note that HPS is equivalent to PLV for a network consisting of two signals. In this case, $M = 2$ and from (8) the direction vector $\Gamma^k(t,\omega) = \left[\gamma^k_1(t,\omega), \gamma^k_2(t,\omega)\right]$, where $\gamma^k_1(t,\omega) = \cos\left(\theta^k_1(t,\omega)\right)$ and $\gamma^k_2(t,\omega) = \sin\left(\theta^k_1(t,\omega)\right)$. Hence, (9) is equivalent to (5).

It can be shown that the HPS defined based on the coordinate system in (8) is dependent on the ordering of the phase differences $\theta_i(t,\omega)$. This dependency will result in unstable HPS values and lead to incorrect interpretation of the multivariate synchrony. To illustrate this problem, we show the derivation of the HPS value for the case of three oscillators $(M = 3)$. The rotating vectors in (8) can be written as,

$$\begin{aligned}
&\gamma^k_1(t,\omega) = \cos\left(\theta^k_1(t,\omega)\right),\\
&\gamma^k_2(t,\omega) = \sin\left(\theta^k_1(t,\omega)\right) \times \cos\left(\theta^k_2(t,\omega)\right),\\
&\gamma^k_3(t,\omega) = \sin\left(\theta^k_1(t,\omega)\right) \times \sin\left(\theta^k_2(t,\omega)\right).
\end{aligned} \tag{10}$$

For simplicity, we further assume that we have only two trials with angular coordinates (or phase differences) $\left\{\theta^1_1(t,\omega), \theta^1_2(t,\omega)\right\}$ and $\left\{\theta^2_1(t,\omega), \theta^2_2(t,\omega)\right\}$, respectively. The corresponding HPS given in (9) reduces to (11) on the following page. In order to show that HPS is dependent on the ordering of the phase differences, we recalculate the HPS with reordered angular coordinates $\left\{\theta^1_2(t,\omega), \theta^1_1(t,\omega)\right\}$ and $\left\{\theta^2_2(t,\omega), \theta^2_1(t,\omega)\right\}$, which in this case reduces to (12) on the bottom of the following page. It is clear that (11) and (12) are not equivalent except in the case of perfect synchrony, i.e., $\theta^1_1(t,\omega) = \theta^1_2(t,\omega), \theta^2_1(t,\omega) = \theta^2_2(t,\omega), \theta^1_1(t,\omega) = \theta^2_1(t,\omega)$ and $\theta^1_2(t,\omega) = \theta^2_2(t,\omega)$. Therefore, the ordering of the phase differences $\theta^k_i(t,\omega)$ plays a major role in calculating the corresponding HPS values. Thus, a modification of this definition

[1]In this paper, unit hyperspheres are sampled based on uniform angular sampling methods in order to generate a suitable set of direction vectors [41].

is required to address this problem. In addition, in order to capture global phase information, we will replace the previously defined pairwise phase differences for HPS by the phase difference between the phase of each oscillator and the phase of the resultant vector of the remaining oscillators [42], given by

$$\theta_i^k(t,\omega) = \Phi_i^k(t,\omega) - \arg\left\{ \sum_{\substack{m=1 \\ m\neq i}}^{M} \exp(j\Phi_m^k(t,\omega)) \right\}. \quad (13)$$

IV. Proposed Solution

A. Hyperspherical Approach

In this section, we propose a solution to the phase ordering problem encountered in HPS. This approach is based on the analysis of the hyperspherical coordinate system given in (8). The coordinates in (8) are equivalent to x coordinates of a rotating circle with varying radii. For example, $\gamma_1^k(t,\omega)$ is the x coordinate of a vector on the unit circle at angular position $\theta_1^k(t,\omega)$, while $\gamma_2^k(t,\omega)$ is the x coordinate of a vector on a circle with radius $\sin\left(\theta_1^k(t,\omega)\right)$ at angular position $\theta_2^k(t,\omega)$. Similar analysis applies to the remaining $\theta_i^k(t,\omega)$s. Thus, every $\gamma_i^k(t,\omega)$ is just the x coordinate of a vector on a circle with radius $r_i(t,\omega) = \prod_{j=1}^{i-1} \sin\left(\theta_j^k(t,\omega)\right)$, for $i = 2,3,\ldots,M$ and with a phase $\theta_i^k(t,\omega)$. The equation for $r_i(t,\omega)$ shows that as i increases, $\gamma_i^k(t,\omega)$ will have less impact on the overall synchrony. This means that the choice of the first phase difference, $\theta_1^k(t,\omega)$, will have a high impact on the measured synchrony.

Equation (8) may also be interpreted as follows. Every $\gamma_i^k(t,\omega)$ is the x projection of the y coordinate of the previous $\gamma_{i-1}^k(t,\omega)$ on the x-axis with a phase $\theta_i^k(t,\omega)$, i.e., define x and y coordinates of the rotating vector for each trial k as

$$\begin{aligned}
\gamma_{x_1}^k(t,\omega) &= \cos\left(\theta_1^k(t,\omega)\right),\\
\gamma_{y_1}^k(t,\omega) &= \sin\left(\theta_1^k(t,\omega)\right),\\
\gamma_{x_2}^k(t,\omega) &= \sin\left(\theta_1^k(t,\omega)\right) \times \cos\left(\theta_2^k(t,\omega)\right),\\
\gamma_{y_2}^k(t,\omega) &= \sin\left(\theta_1^k(t,\omega)\right) \times \sin\left(\theta_2^k(t,\omega)\right),\\
\gamma_{x_3}^k(t,\omega) &= \sin\left(\theta_1^k(t,\omega)\right) \times \sin\left(\theta_2^k(t,\omega)\right)\\
&\quad \times \cos\left(\theta_3^k(t,\omega)\right),\\
\gamma_{y_3}^k(t,\omega) &= \sin\left(\theta_1^k(t,\omega)\right) \times \sin\left(\theta_2^k(t,\omega)\right)\\
&\quad \times \sin\left(\theta_3^k(t,\omega)\right),\\
&\vdots\\
\gamma_{x_M}^k(t,\omega) &= \sin\left(\theta_1^k(t,\omega)\right) \times \cdots \times \sin\left(\theta_{M-1}^k(t,\omega)\right)\\
&\quad \times \cos\left(\theta_M^k(t,\omega)\right),\\
\gamma_{y_M}^k(t,\omega) &= \sin\left(\theta_1^k(t,\omega)\right) \times \cdots \times \sin\left(\theta_{M-1}^k(t,\omega)\right)\\
&\quad \times \sin\left(\theta_M^k(t,\omega)\right), \qquad (14)
\end{aligned}$$

where the phases $\theta_i^k(t,\omega)$s are defined as in (13) and the superscripts x and y refer to the projection coordinates.

We can also rewrite (14) as,

$$\begin{aligned}
\gamma_{x_1}^k(t,\omega) &= \cos\left(\theta_1^k(t,\omega)\right),\\
\gamma_{x_2}^k(t,\omega) &= \gamma_{y_1}^k(t,\omega) \times \cos\left(\theta_2^k(t,\omega)\right),\\
\gamma_{x_3}^k(t,\omega) &= \gamma_{y_2}^k(t,\omega) \times \cos\left(\theta_3^k(t,\omega)\right),\\
&\vdots\\
\gamma_{x_M}^k(t,\omega) &= \gamma_{y_{M-1}}^k(t,\omega) \times \cos\left(\theta_M^k(t,\omega)\right),\\
\gamma_{y_M}^k(t,\omega) &= \gamma_{y_{M-1}}^k(t,\omega) \times \sin\left(\theta_M^k(t,\omega)\right). \qquad (15)
\end{aligned}$$

Equation (15) reveals that the radius $r_i^k(t,\omega) = \prod_{j=1}^{i-1} \sin\left(\theta_j^k(t,\omega)\right)$, for $i = 2,3,\ldots,M$ is just the y coordinate of the previous $\gamma_{y_{i-1}}^k(t,\omega)$. This recursive structure is the cause of the ordering problem. To solve this problem, we propose to consider both the x and y coordinates for all oscillators.

By computing the l_2 norm, $d_i^k(t,\omega)$, of the direction vectors for each oscillator i using the coordinates $\gamma_{x_i}^k(t,\omega)$ and $\gamma_{y_i}^k(t,\omega)$, we end up with the following norms,

$$\begin{aligned}
d_1^k(t,\omega) &= 1,\\
d_2^k(t,\omega) &= \sin\left(\theta_1^k(t,\omega)\right),\\
d_3^k(t,\omega) &= \sin\left(\theta_1^k(t,\omega)\right) \times \sin\left(\theta_2^k(t,\omega)\right),\\
&\vdots\\
d_M^k(t,\omega) &= \sin\left(\theta_1^k(t,\omega)\right) \times \cdots \times \sin\left(\theta_{M-1}^k(t,\omega)\right), \qquad (16)
\end{aligned}$$

or simply $d_i^k(t,\omega) = r_i^k(t,\omega) = \prod_{j=1}^{i-1} \sin\left(\theta_j^k(t,\omega)\right)$ for $i = 2,3,\ldots,M$. Thus, in order to get rid of the dependency on the phase ordering, we propose to normalize $\gamma_{x_i}^k(t,\omega)$ and $\gamma_{y_i}^k(t,\omega)$ by $d_i^k(t,\omega)$. This will result in unit radius for all i. Therefore, the modified multivariate phase synchrony measure is given by

$$\mathrm{HPS}(t,\omega) = \frac{1}{N \times \sqrt{M}} \left\| \sum_{k=1}^{N} D^k(t,\omega) \right\|_2, \qquad (17)$$

where

$$D^k(t,\omega) = \left[\frac{\gamma_{x_1}^k(t,\omega)}{d_1^k(t,\omega)}, \frac{\gamma_{y_1}^k(t,\omega)}{d_1^k(t,\omega)}, \ldots, \frac{\gamma_{x_M}^k(t,\omega)}{d_M^k(t,\omega)}, \frac{\gamma_{y_M}^k(t,\omega)}{d_M^k(t,\omega)} \right].$$

$$\begin{aligned}
\mathrm{HPS}(t,\omega) &= \frac{1}{N}\sqrt{\left(\sum_{k=1}^{N}\gamma_1^k(t,\omega)\right)^2 + \left(\sum_{k=1}^{N}\gamma_2^k(t,\omega)\right)^2 + \left(\sum_{k=1}^{N}\gamma_3^k(t,\omega)\right)^2}\\
&= \frac{1}{2}\sqrt{2 + 2\cos\left(\theta_1^1(t,\omega)\right)\cos\left(\theta_1^2(t,\omega)\right) + 2\sin\left(\theta_1^1(t,\omega)\right)\sin\left(\theta_1^2(t,\omega)\right)\cos\left(\theta_2^1(t,\omega) - \theta_2^2(t,\omega)\right)}. \qquad (11)\\
\mathrm{HPS}(t,\omega) &= \frac{1}{2}\sqrt{2 + 2\cos\left(\theta_2^1(t,\omega)\right)\cos\left(\theta_2^2(t,\omega)\right) + 2\sin\left(\theta_2^1(t,\omega)\right)\sin\left(\theta_2^2(t,\omega)\right)\cos\left(\theta_1^1(t,\omega) - \theta_1^2(t,\omega)\right)}. \qquad (12)
\end{aligned}$$

As the l_2 norm of each vector $D^k(t,\omega)$ in the above equation is equal to $\sqrt{M}$, to make the definition and range of HPS consistent with PLV (see (5)) we normalize HPS by $\sqrt{M}$.

The modified measure given in (17) can be rewritten as in (18) at the bottom of the page. By noting that $\cos\left(\theta_i^k(t,\omega)\right) = \frac{\gamma_{x_i}^k(t,\omega)}{d_i^k(t,\omega)}$ and $\sin\left(\theta_i^k(t,\omega)\right) = \frac{\gamma_{y_i}^k(t,\omega)}{d_i^k(t,\omega)}$ we can write the modified HPS as

$$\begin{aligned}\mathrm{HPS}(t,\omega) &= \frac{1}{\sqrt{M}}\sqrt{\mathrm{PLV}_1^2(t,\omega)+\cdots+\mathrm{PLV}_M^2(t,\omega)} \\ &= \sqrt{\frac{1}{M}\sum_{i=1}^{M}\mathrm{PLV}_i^2(t,\omega)}, \end{aligned} \tag{19}$$

where PLV_i^2 quantifying the synchronization of each oscillator with respect to a common reference angle with $\theta_i^k(t,\omega)$ as defined in (13) and PLV_i is given by

$$\begin{aligned}\mathrm{PLV}_i(t,\omega) &= \frac{1}{N}\left|\sum_{k=1}^{N}\exp\left(j\theta_i^k(t,\omega)\right)\right| \\ &= \sqrt{\left\langle\cos\theta_i^k(t,\omega)\right\rangle^2+\left\langle\sin\theta_i^k(t,\omega)\right\rangle^2}. \end{aligned} \tag{20}$$

The maximum value of $\mathrm{HPS}(t,\omega)$ is 1, when there is complete phase synchronization among oscillators. On the other hand, $\mathrm{HPS}(t,\omega)$ is theoretically 0 when the oscillators are independent.

B. Hyper-Torus Synchrony

Results found in the previous section can alternatively be derived from an alternative mapping: the Cartesian product of unit circles parameterized by phase differences as given in (13). In a network consisting of M oscillators, consider a phase $\theta_i^k(t,\omega)$ that parameterizes the unit circle $\mathbb{S}^1 \subset \mathbb{R}^2$ by the angular coordinates $\mathbb{S}^1 = \left\{\left(\cos\left(\theta_i^k\right),\sin\left(\theta_i^k\right)\right) \mid 0 \le \theta_i^k \le 2\pi\right\}$. Let another unit circle $\mathbb{S}^1 \subset \mathbb{R}^2$ be parameterized by the angular coordinates $\mathbb{S}^1 = \left\{\left(\cos\left(\theta_j^k\right),\sin\left(\theta_j^k\right)\right) \mid 0 \le \theta_j^k \le 2\pi\right\}$. The Cartesian product $\mathbb{S}^1\times\mathbb{S}^1$ defines the manifold $\mathbb{T}^2 = \mathbb{S}^1\times\mathbb{S}^1 = \left\{\left(\cos\left(\theta_i^k\right),\cos\left(\theta_j^k\right),\sin\left(\theta_i^k\right),\sin\left(\theta_j^k\right)\right) \mid 0 \le \theta_i^k,\theta_j^k \le 2\pi\right\}$ embedded in $\mathbb{R}^4$. The M-dimensional flat torus $\mathbb{T}^m \subset \mathbb{R}^{2m}$ is the manifold $\mathbb{T}^m = \mathbb{S}^1\times\cdots\times\mathbb{S}^1$ defined by $x_1^2+y_1^2 = \cdots = x_M^2+y_M^2 = 1$. It is parameterized by $x_i = \cos\left(\theta_i(t,\omega)\right)$ and $y_i = \sin\left(\theta_i(t,\omega)\right)$ [43].

A Riemannian metric g on a n-dimensional manifold M defines an inner product between tangent vectors in each tangent space T_pM for every point $p \in M$ [43]. A Riemannian manifold (M,g) is a differentiable manifold equipped with a Riemannian metric [44]. Thus, for every point p in (M,g) the length of any tangent vector $X \in T_pM$ is given by $|X| = \langle X,X\rangle^{1/2}$ [43]. The Cartesian product between two Riemannian manifolds (M_1,g_1) and (M_2,g_2) is equipped with the product metric $g = g_1 \oplus g_2$, which is defined as [43]

$$g(X_1+X_2,Y_1+Y_2) = g(X_1+Y_1)+g(X_2+Y_2), \tag{21}$$

where $X_i, Y_i \in T_{p_i}M_i$ and $T_{(p_1,p_2)}\ (M_1\times M_2) = T_{p_1}M_1 \oplus T_{p_2}M_2$.

A torus $\mathbb{T}^m$ is locally isometric to Euclidean space, meaning that every point on $\mathbb{T}^m$ has a neighborhood that is isometric to an open set in $\mathbb{R}^m$ [43], which results in a manifold whose curvature is zero everywhere and its tangent spaces are identical to the manifold [45]. Hence, $\mathbb{T}^m$ is a flat Riemannian manifold equipped with the Euclidean metric [46].

For a group of M oscillators, vector (22) lies in $\mathbb{T}^m$

$$\Gamma^k(t,\omega) = \left[x_1^k, y_1^k, \ldots, x_M^k, y_M^k\right], \tag{22}$$

where $x_i^k = \cos\left(\theta_i^k(t,\omega)\right), y_i^k = \sin\left(\theta_i^k(t,\omega)\right)$, and $\theta_i^k(t,\omega)$ is a phase difference as defined in (13) for the kth trial.

$\mathrm{HTS}(t,\omega)$ can then be defined as

$$\mathrm{HTS}(t,\omega) = \frac{1}{N\sqrt{M}}\left\|\sum_{k=1}^{N}\Gamma^k(t,\omega)\right\|_2, \tag{23}$$

where M is the number of oscillators and N is the total number of trials. HTS can be re-expressed as shown in (24) at the bottom of the following page, which is equivalent to (19). Throughout the rest of this article we will use HTS to refer to both approaches.

C. Computational Complexity

HTS involves the computation of M PLVs, with complexity $\mathcal{O}(M\ \log\ n)$ per time-frequency point [47], where n is the number of points used in the fast Fourier transforms (ffts) in the computation of the time-frequency distribution (usually equal or greater than the length of the signal). The computation of one square root has complexity $\mathcal{O}(m^2)$ when computed through the Newton-Raphson Method [48], where m corresponds to the minimum of the number of bits from the two numbers being multiplied (32 or 64 bits for double precision). Thus, the total computational complexity of HTS is $\mathcal{O}(M\ \log\ n)+\mathcal{O}(m^2)$. On the other hand, the computational complexity of the S-estimator relies on the computation of $\left(\binom{M}{2}\right)$ PLVs for the construction of the synchronization matrix and its eigendecomposition. Computing $\left(\binom{M}{2}\right)$ PLVs has a complexity of $\mathcal{O}\left(\left(\binom{M}{2}\right)\log\ n\right)$, which can be approximated as $\mathcal{O}(\frac{M}{2}\log n)$ for large M. The eigendecomposition of the synchronization matrix has complexity $\mathcal{O}(M^3)$ [49]. Thus, the total computational complexity of the S-estimator is $\mathcal{O}(\frac{M}{2}\log n)+\mathcal{O}(M^3)$. Therefore, the proposed metric is computationally more efficient than the S-estimator.

$$\mathrm{HPS}(t,\omega) = \frac{1}{N\sqrt{M}}\sqrt{\left(\sum_{k=1}^{N}\frac{\gamma_{x_1}^k(t,\omega)}{d_1^k(t,\omega)}\right)^2+\left(\sum_{k=1}^{N}\frac{\gamma_{y_1}^k(t,\omega)}{d_1^k(t,\omega)}\right)^2+\cdots+\left(\sum_{k=1}^{N}\frac{\gamma_{x_M}^k(t,\omega)}{d_M^k(t,\omega)}\right)^2+\left(\sum_{k=1}^{N}\frac{\gamma_{y_M}^k(t,\omega)}{d_M^k(t,\omega)}\right)^2}. \tag{18}$$

V. Statistical Assessment of HTS

In this section, we assessed the asymptotic properties of the expected value and variance of $\widehat{\mathrm{HTS}}(t,\omega)$ in the absence of synchrony as well as for different levels of synchrony. Finally, as previously done for PLV, we found an unbiased estimator for $\widehat{\mathrm{HTS}}^2$ and evaluated its variance empirically.

A. Bias

Due to its dependence on PLV, the proposed measure also exhibits a bias which is dependent on the number of trials. We will first illustrate this dependency by assuming a Von Mises distribution for phase differences. The Von Mises distribution $\mathrm{VM}(\theta,\kappa)$ is the most common model for circular data [42]. It is defined by the reference direction, θ, and its dispersion about that direction, κ. Its probability density function is given by

$$f(\theta) = [2\pi I_0(\kappa)]^{-1} \exp\left[\kappa\cos(\theta-\mu)\right], \quad 0 \le \theta < 2\pi,\ 0 \le \kappa < \infty, \tag{25}$$

where $I_0(\kappa) = (2\pi)^{-1}\int_0^{2\pi} \exp\left[\kappa\cos(\phi-\mu)\right]$ is the modified Bessel function of order zero [42].

Fig. 1 illustrates the theoretical and experimental multivariate synchrony, HTS and $\widehat{\mathrm{HTS}}$, respectively, for different levels of synchronization in a network consisting of $M = 4$ oscillators. Here we are assuming that the phase differences in (19) and (24) are equally distributed according to $\mathrm{VM}(0,\kappa)$ for simplicity and various levels of synchrony are obtained by varying the concentration parameter κ. As observed, the bias of HTS depends on the underlying distribution of the angles θ_i, bias being the most prominent in the absence of synchrony, or when θ_i is uniformly distributed. In addition, the bias is dependent on the sample size and results based on small sample sizes should be interpreted carefully.

In this paper, we further assessed the bounds on the bias and variance of $\widehat{\mathrm{HTS}}$. A lower bound on bias can be found from the inequality for arithmetic and quadratic means [50] as

$$\frac{\mathrm{PLV}_1(t,\omega)+\cdots+\mathrm{PLV}_M(t,\omega)}{M} \le \sqrt{\frac{\mathrm{PLV}_1^2(t,\omega)+\cdots+\mathrm{PLV}_M^2(t,\omega)}{M}}, \tag{26}$$

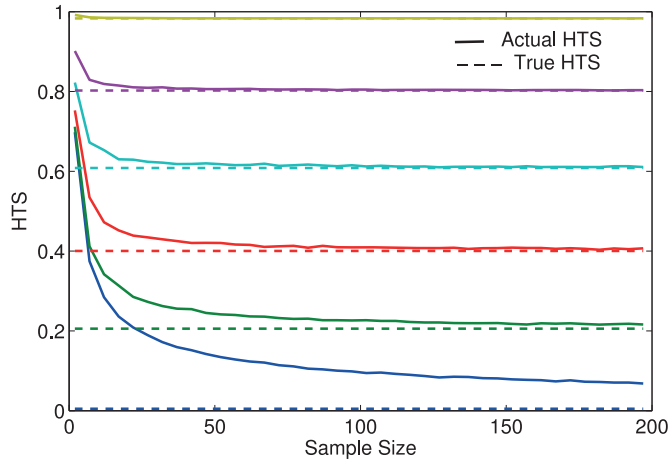

Fig. 1. $\widehat{\mathrm{HTS}}$ (solid lines) and true HTS (dashed lines) for synchrony values of 0, 0.20, 0.40, 0.60, 0.80 and 0.99. $M = 4$ oscillators were simulated with phases θ_i distributed as $\mathrm{VM}(0,\kappa)$.

where the absolute value in the original inequality is no longer required since $\widehat{\mathrm{PLV}}(t,\omega) \in [0,1]$. An upper bound can be found as

$$\sqrt{\frac{\mathrm{PLV}_1^2(t,\omega)+\cdots+\mathrm{PLV}_M^2(t,\omega)}{M}} \le \frac{\mathrm{PLV}_1(t,\omega)+\cdots+\mathrm{PLV}_M(t,\omega)}{\sqrt{M}}. \tag{27}$$

Thus, the lower and upper bounds on the expected value of $\widehat{\mathrm{HTS}}(t,\omega)$ can be found as

$$\begin{aligned} E\left[\widehat{\mathrm{HTS}}(t,\omega)\right] &= E\left[\sqrt{\frac{1}{M}\sum_{i=1}^{M}\widehat{\mathrm{PLV}}_i^2(t,\omega)}\right] \\ &\ge E\left[\frac{1}{M}\sum_{i=1}^{M}\widehat{\mathrm{PLV}}_i(t,\omega)\right] \\ &= \frac{1}{M}\sum_{i=1}^{M} E\left[\widehat{\mathrm{PLV}}_i(t,\omega)\right], \end{aligned} \tag{28}$$

and

$$E\left[\widehat{\mathrm{HTS}}(t,\omega)\right] \le E\left[\frac{1}{\sqrt{M}}\sum_{i=1}^{M}\widehat{\mathrm{PLV}}_i(t,\omega)\right], \tag{29}$$

respectively.

$$\begin{aligned} \mathrm{HTS}(t,\omega) &= \frac{1}{N\sqrt{M}}\sqrt{\left(\sum_{k=1}^{N}\cos\theta_1^k(t,\omega)\right)^2+\left(\sum_{k=1}^{N}\sin\theta_1^k(t,\omega)\right)^2+\cdots+\left(\sum_{k=1}^{N}\cos\theta_M^k(t,\omega)\right)^2+\left(\sum_{k=1}^{N}\sin\theta_M^k(t,\omega)\right)^2} \\ &= \frac{1}{\sqrt{M}}\sqrt{\langle\cos\theta_1^k(t,\omega)\rangle^2+\langle\sin\theta_1^k(t,\omega)\rangle^2+\cdots+\langle\cos\theta_M^k(t,\omega)\rangle^2+\langle\sin\theta_M^k(t,\omega)\rangle^2} \\ &= \frac{1}{\sqrt{M}}\sqrt{\mathrm{PLV}_1^2(t,\omega)+\cdots+\mathrm{PLV}_M^2(t,\omega)} \\ &= \sqrt{\frac{1}{M}\sum_{i=1}^{M}\mathrm{PLV}_i^2(t,\omega)}, \end{aligned} \tag{24}$$

An approximate value for $E\left[\widehat{\mathrm{PLV}}(t,\omega)\right]$ in the absence of synchrony has been previously found to be $E\left[\widehat{\mathrm{PLV}}(t,\omega)\right] \approx \frac{1}{\sqrt{N}}$ [19]. Hence, $E\left[\widehat{\mathrm{HTS}}(t,\omega)\right]$ can be bounded as

$$\frac{1}{\sqrt{N}} \leq E\left[\widehat{\mathrm{HTS}}(t,\omega)\right] \leq \sqrt{\frac{M}{N}}. \tag{30}$$

Equation (30) shows that in a network in which all oscillators are independent, the minimum possible value that $\widehat{\mathrm{HTS}}$ can attain is inversely proportional to the square root of the total number of trials or observations, as previously found for $\widehat{\mathrm{PLV}}$. On the other hand, its upper bound is directly proportional to the number of oscillators.

Asymptotic results for $E\left[\widehat{\mathrm{PLV}}(t,\omega)\right]$, or the mean resultant length as known in the circular statistics community, have been found for the Von Mises distribution with mean direction $\theta = 0$ and concentration parameter $\kappa > 0$ [51] as

$$E\left[\widehat{\mathrm{PLV}}(t,\omega)\right] = A(\kappa) + \frac{1}{2N\kappa}, \tag{31}$$

where $A(\kappa) = \frac{I_1(\kappa)}{I_0(\kappa)}$ and $I_i(\kappa)$ is the modified Bessel function of the first kind of the ith order. Considering all M oscillator's θ_is to be identically distributed and substituting (31) into (28) and (29) yields

$$\left(A(\kappa) + \frac{1}{2N\kappa}\right) \leq E\left[\widehat{\mathrm{HTS}}(t,\omega)\right] \leq \sqrt{M}\left(A(\kappa) + \frac{1}{2N\kappa}\right). \tag{32}$$

B. Variance

In order to find an upper bound on the variance of $\widehat{\mathrm{HTS}}(t,\omega)$ we will define $\widehat{\mathrm{HTS}}^2(t,\omega)$ as

$$\widehat{\mathrm{HTS}}^2(t,\omega) = \frac{1}{M}\sum_{i=1}^{M} \widehat{\mathrm{PLV}}_i^2(t,\omega). \tag{33}$$

Taking expectation on both sides yields

$$E\left[\widehat{\mathrm{HTS}}^2(t,\omega)\right] = E\left[\frac{1}{M}\sum_{i=1}^{M} \widehat{\mathrm{PLV}}_i^2(t,\omega)\right] = \frac{1}{M}\sum_{i=1}^{M} E\left[\widehat{\mathrm{PLV}}_i^2(t,\omega)\right], \tag{34}$$

where the linearity property of expectation has been employed. The expected value of $\widehat{\mathrm{PLV}}^2(t,\omega)$ is a well known expression [51], [52], given by

$$E\left[\widehat{\mathrm{PLV}}_i^2(t,\omega)\right] = \frac{1}{N} + \left(1 - \frac{1}{N}\right)\mathrm{PLV}_i^2(t,\omega). \tag{35}$$

Thus, substituting (35) in (34) yields

$$E\left[\widehat{\mathrm{HTS}}^2(t,\omega)\right] = \frac{1}{N} + \left(1 - \frac{1}{N}\right)\mathrm{HTS}^2(t,\omega). \tag{36}$$

An upper bound on the variance of $\widehat{\mathrm{HTS}}(t,\omega)$ in the absence of synchrony can be found as

$$\begin{aligned} Var\left(\widehat{\mathrm{HTS}}(t,\omega)\right) &= E\left[\widehat{\mathrm{HTS}}^2(t,\omega)\right] - E\left[\widehat{\mathrm{HTS}}(t,\omega)\right]^2 \\ &\leq \frac{1}{N} + \left(1 - \frac{1}{N}\right)\mathrm{HTS}^2(t,\omega) - \left(\frac{1}{\sqrt{N}}\right)^2 \\ &= 1 - \frac{1}{N}\mathrm{HTS}^2(t,\omega). \end{aligned} \tag{37}$$

Thus, in the absence of synchrony, the maximum possible value that the variance of $\widehat{\mathrm{HTS}}$ can attain is 1.

In the case of $\mathrm{VM}(0,\theta)$ the upper bound for the variance is

$$\mathrm{Var}\left(\widehat{\mathrm{HTS}}(t,\omega)\right) \leq \left(\frac{1}{N} + \left(1 - \frac{1}{N}\right)\mathrm{HTS}^2(t,\omega)\right) - \left(A^2(\kappa) + 2A(\kappa)\frac{1}{2N\kappa} + \frac{1}{4N^2\kappa^2}\right). \tag{38}$$

where phase differences θ_i are drawn from $\mathrm{VM}(0,\kappa)$.

Fig. 2(a) and (b) show the upper bounds on the variance of $\widehat{\mathrm{HTS}}(t,\omega)$ and its empirical variance, respectively, for various levels of synchrony in a network consisting of $M = 4$ oscillators. From Fig. 2(a), the variance of $\widehat{\mathrm{HTS}}(t,\omega)$ decreases as the number of trials or observations increase as well as when the global synchronization increases. Fig. 2(b) shows the variance of $\widehat{\mathrm{HTS}}(t,\omega)$ obtained empirically for various levels of synchrony. It is observed that the empirical variance follows similar trends as those obtained by the upper bound, without attaining it.

C. Correction of Bias in $\widehat{\mathrm{HTS}}^2$

As in the case of PLV [52], [53], it is straightforward to find an unbiased estimator of $\widehat{\mathrm{HTS}}^2(t,\omega)$ rather than for $\widehat{\mathrm{HTS}}(t,\omega)$. Equation (36) suggests that the bias in $\widehat{\mathrm{HTS}}$ arises from the bias in $\widehat{\mathrm{PLV}}$. An unbiased estimator for $\widehat{\mathrm{HTS}}^2(t,\omega)$ can be found as

$$\widehat{\mathrm{HTS}}^2_{\mathrm{UB}}(t,\omega) = \frac{1}{N-1}\left(\widehat{\mathrm{HTS}}^2(t,\omega) \times N - 1\right). \tag{39}$$

This result is obtained similarly by substituting $\widehat{\mathrm{PLV}}^2(t,\omega)$ in (34) by its unbiased estimator previously found in [52], [53]

$$\begin{aligned} \widehat{\mathrm{PLV}}^2_{i(\mathrm{UB})}(t,\omega) &= \frac{2}{N(N-1)} \times \sum_{n=1}^{N-1}\sum_{m=n+1}^{N} \cos\left(\phi_i^m(t,\omega) - \phi_i^n(t,\omega)\right) \\ &= \frac{1}{N-1}\left(\widehat{\mathrm{PLV}}_i^2(t,\omega) \times N - 1\right). \end{aligned} \tag{40}$$

Figs. 3 and 4 illustrate the expected value and variance of $\widehat{\mathrm{HTS}}^2(t,\omega)$ and $\widehat{\mathrm{HTS}}^2_{\mathrm{UB}}(t,\omega)$ for various synchrony values. As previously reported for $\widehat{\mathrm{PLV}}^2$, the variance of the unbiased estimator is slightly higher than that of the biased estimator for small sample sizes.

VI. Results

In this section, results of multivariate phase synchronization on simulated and real data are presented. First, the proposed measure is evaluated on a network of Kuramoto oscillators with

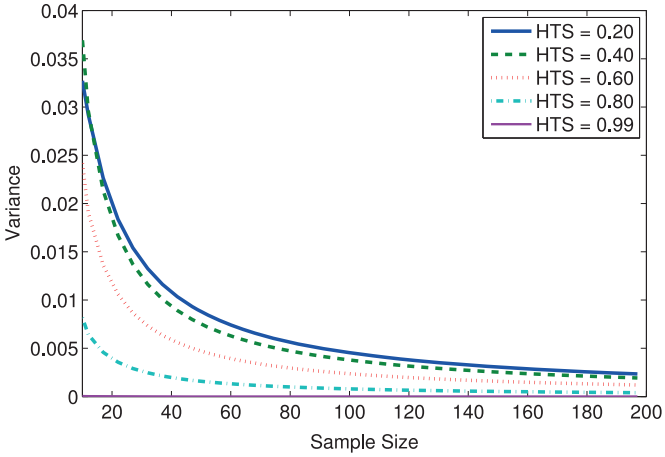

(a)

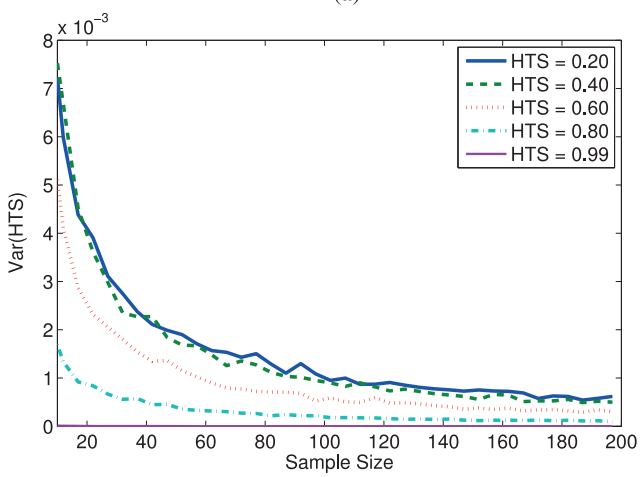

(b)

Fig. 2. (a) Theoretical upper bounds for the variance of HTS; and (b) empirical variance of HTS as a function of sample size in a network of M = 4 oscillators for different synchronization levels in the Von Mises distribution in (38). (a) Upper bounds for variance of $\widehat{\mathrm{HTS}}(t,\omega)$. (b) Empirical variance of $\widehat{\mathrm{HTS}}(t,\omega)$.

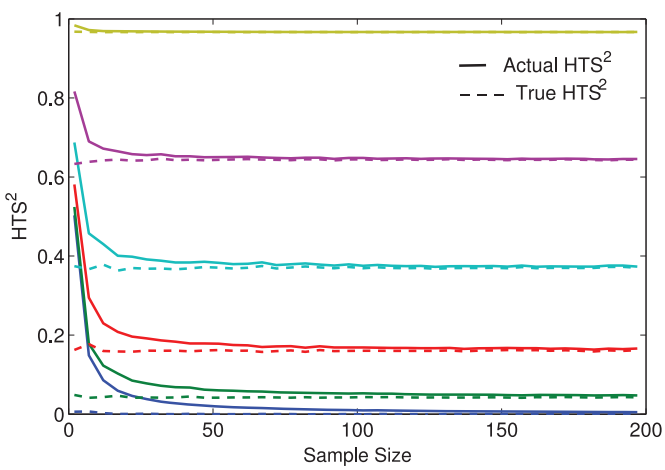

Fig. 3. $\widehat{\mathrm{HTS}}^2$ (solid lines) and true HTS^2 (dashed lines) for true HTS values of 0, 0.20, 0.40, 0.60, 0.80 and 0.99.

varying coupling strengths. Next, the sensitivity to global coupling is evaluated for various Rössler oscillators. Finally, the

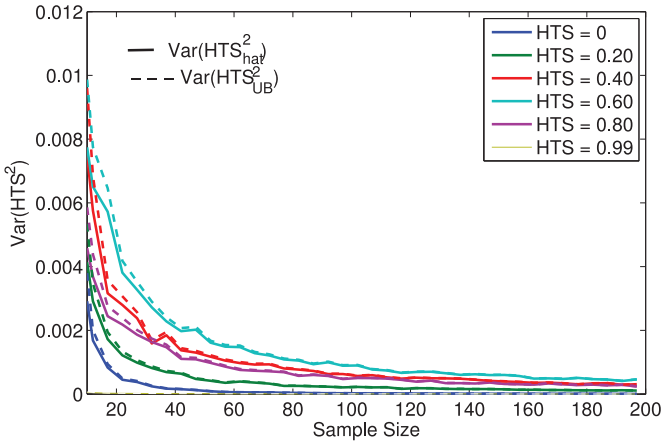

Fig. 4. Variance of $\widehat{\mathrm{HTS}}^2$ (solid lines) and true HTS^2 (dashed lines) for true HTS values of 0, 0.20, 0.40, 0.60, 0.80 and 0.99.

proposed measure is implemented in the assessment of multivariate synchrony in a EEG dataset.

A. Kuramoto Model

In order to evaluate the performance of the proposed measure as a function of coupling strength, we computed the multivariate synchrony in a large network of coupled oscillators as presented by Kuramoto [54]. Kuramoto model describes a system consisting of multiple oscillators with different natural frequencies which synchronize to a common frequency after their coupling exceeds a certain threshold [55]. This model has been used to describe many physical phenomena, ranging from unicellular organisms [56] to the neurosciences [20], [57]. Phase dynamics governing the cooperative synchronization among M oscillators are given by

$$\frac{d\phi_i}{dt} = \omega_i + \frac{K}{M}\sum_{j=1}^{M}\sin(\phi_j - \phi_i), \tag{41}$$

where ϕ_i corresponds to the phase of the ith oscillator, ω_i is its natural frequency and K corresponds to the coupling strength, which is equal among all oscillators. The natural frequency of each oscillator is chosen randomly from a Lorentzian distribution given by

$$g(\omega) = \frac{\gamma}{\pi\left[\gamma^2 + (\omega - \omega_o)^2\right]}, \tag{42}$$

with mean ω_o and width γ.

Kuramoto found that oscillators are desynchronized until K exceeds a critical value $K_c = 2\gamma$. Exceeding K_c separates the oscillators into two groups: one that contributes to the synchronization of the system and another whose natural frequencies come from the tails of the distribution and contribute to desynchronization of the system [58]. As K increases, the group of synchronized oscillators increases until all oscillators are synchronized. A network consisting of $M = 64$ oscillators was simulated and the time-varying phases $\phi_i(t)$ were solved numerically via Runge-Kutta with a time step of $\Delta t = 0.0078$ s, which results in a sampling frequency of 128 Hz. The natural

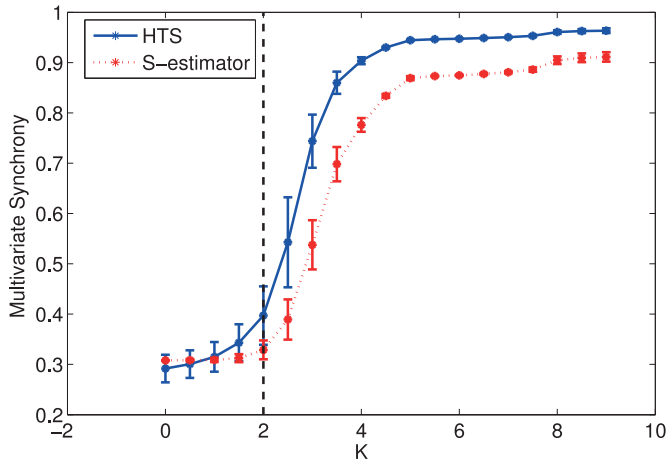

Fig. 5. Comparison of mean and standard deviation of multivariate synchrony (HTS and S-estimator) within a Kuramoto network with $K_c = 2$.

frequencies of each oscillator are drawn from a Lorentzian distribution as given by (42) where $\omega_o = 40$ rad/s and $\gamma = 1$. This results in a $K_c = 2\gamma = 2$. The signal length was 2048 samples, and the first 500 samples were discarded to avoid transients.

Fig. 5 shows multivariate synchrony estimated from HTS and the S-estimator as K increased from 0 to 9 in increments of 0.5. We expect to observe low synchrony for $K < K_c$ with a sudden increase in synchrony after K_c. When $K = 0$ multivariate synchrony from both S-estimator and HTS is greater than 0, which indicates bias on the estimators when phases come from an uniform distribution. On the other hand, HTS is more sensitive to the increase of global synchronization for $K = K_c = 2$ compared to the S-estimator. The standard deviation of both estimators is maximal around K_c [57], with S-estimator showing less variance than HTS since it is a weighted average of all bivariate PLVs, obtained from the eigendecomposition. Finally, when the system is fully synchronized HTS approaches 1 as expected.

B. Rössler Oscillator

In order to test multivariate synchrony under different network configurations we used a Rössler oscillator model. Rössler oscillators describe a system of weakly coupled self-sustained stochastic oscillators [59]. We modeled a network consisting of 6 oscillators coupled through their x-dimension [60]. Eight different configurations are considered, illustrated in Fig. 6. It is expected that networks 1 and 2 will exhibit low synchrony, and network 8 will result in multivariate synchrony close to 1. Dynamics governing the networks under study are given by

$$\dot{\xi}_j = \begin{pmatrix} \dot{X}_j \\ \dot{Y}_j \\ \dot{Z}_j \end{pmatrix} = \begin{pmatrix} \dot{X}_j = -\omega_j Y_j - Z_j + \left[\sum_{i \neq j} \epsilon_{ij}(X_i - X_j)\right] + \sigma\eta_j \\ \dot{Y}_j = -\omega_j X_j - a Y_j \\ \dot{Z}_j = b + (X_j - c) Z_j \end{pmatrix}, \tag{43}$$

where $i, j = 1, 2, \ldots, 6$, $a = 0.35$, $b = 0.2$, $c = 10, \omega_1 = 1.05, \omega_2 = 1.03, \omega_3 = 1.01, \omega_4 = 0.99, \omega_5 = 0.97, \omega_6 = 0.95, \varepsilon_{ij} = \varepsilon_{ji} = 0.5, \sigma = 1.5$ and η_j is white Gaussian noise. The differential equations were solved by the Runge-Kutta method at a time step of 0.067 seconds. Simulations were repeated 200 times, for a signal length of 2000 samples and sampling frequency of 15 Hz.

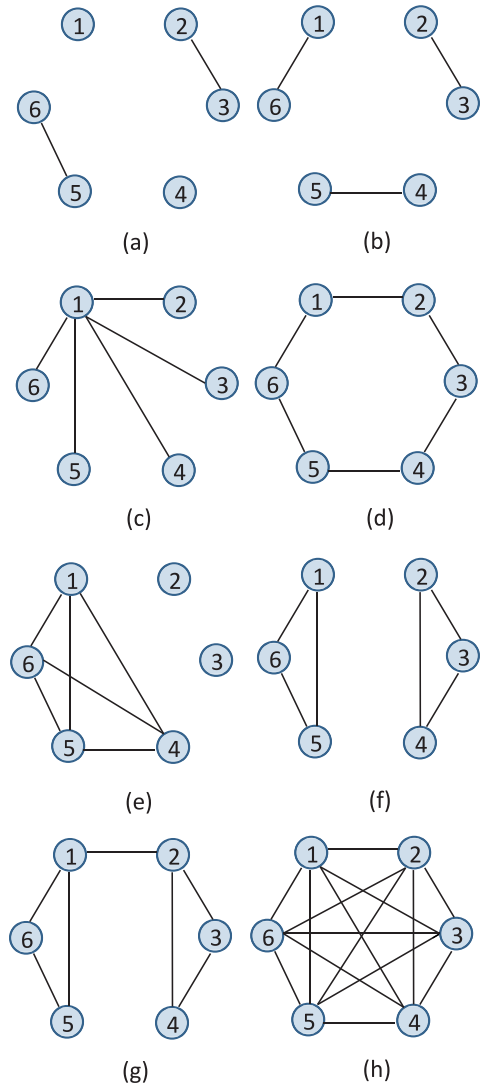

Fig. 6. Eight Rössler networks. (a) Network 1, (b) Network 2, (c) Network 3, (d) Network 4, (e) Network 5, (f) Network 6, (g) Network 7 (h) Network 8.

Table I compares multivariate synchrony evaluated using HTS and S-estimator for each of the eight Rössler networks presented in Fig. 6. The second and third columns show results for HTS and S-estimator (mean±st.dev.) computed according to (23) and (6), respectively. Multivariate synchrony values obtained from both measures are comparable and align with our expectations for all networks. For both methods, the multivariate synchrony results for each network is significantly different from that obtained from a null network in which none of the oscillators is connected, i.e., $\varepsilon_{ij} = 0$, (Wilcoxon rank sum test, $p < 0.01$).

The two networks differ in their behavior only for networks 5 and 6. In the case of network 5, multivariate synchrony obtained from HTS is higher than that from network 6, whereas it is the opposite for S-estimator. In network 5, four out of six

TABLE I
MULTIVARIATE SYNCHRONY (MEAN±ST.DEV.) IN NETWORKS OF RÖSSLER OSCILLATORS

Network	HTS	S	HTS^2_{UB}	S^2_{UB}
1	0.226±0.023	0.267±0.004	0.051±0.010	0.254±0.002
2	0.612±0.028	0.474±0.016	0.375±0.034	0.384±0.009
3	0.944±0.029	0.851±0.059	0.892±0.055	0.765±0.086
4	0.985±0.000	0.945±0.001	0.971±0.000	0.907±0.001
5	0.800±0.009	0.580±0.012	0.640±0.015	0.523±0.007
6	0.765±0.027	0.673±0.011	0.586±0.042	0.610±0.005
7	0.980±0.001	0.929±0.002	0.960±0.002	0.881±0.004
8	0.999±0.000	0.996±0.000	0.998±0.000	0.993±0.000

TABLE II
MULTIVARIATE SYNCHRONY (MEAN±ST.DEV.) FOR DIFFERENT NUMBER OF OSCILLATORS CONTAINING TWO SUBNETWORKS OF THREE OSCILLATORS

Number of Oscillators	HTS	S	HTS^2_{UB}	S^2_{UB}
6	0.765±0.027	0.673±0.011	0.585±0.042	0.610±0.005
9	0.682±0.017	0.457±0.011	0.463±0.024	0.372±0.009
12	0.613±0.015	0.348±0.008	0.373±0.018	0.263±0.006

oscillators are all interconnected with only two isolated oscillators contributing to low synchrony. Since HTS relies on the root mean square of PLVs with one PLV computed between each oscillaor and the mean phase, there will be only two PLVs with low synchrony. On the other hand, in network 6 although there are two sub-networks that are fully synchronized these are not interconnected and hence the global synchrony of the network should not be as high as in network 5 as indicated by HTS. This result is also observed from the unbiased squared HTS and S-estimator, as shown in the fourth and fifth columns of Table I, respectively. Here, $\mathrm{HTS}^2_{\mathrm{UB}}$ is computed as in (39) and S^2_{UB} is obtained by using unbiased PLV^2 as in (40). Note that network 4 also contains 6 connections and results in higher synchrony than networks 5 and 6. This is due to the indirect connections that emerge when oscillators are interconnected through a third oscillator.

In order to assess the effect of the number of oscillators in the computed synchrony values, we constructed two subnetworks consisting of 3 oscillators each (as in Fig. 6(f)) and increased the number of oscillators in the network to 9 and 12. Table II shows the results for both HTS and S-estimator as the number of oscillators increases. Note that the first case, 6 oscillators, is the same as network 6 in Fig. 6. For both methods, as the number of oscillators increases the multivariate synchrony decreases as there are more non-synchronized oscillators in the network. This trend is also observed from the unbiased estimators of HTS^2 and S^2.

Finally, we assessed the effect of the number of subnetworks on the multivariate synchrony measures. Table III shows the results for HTS, S, their squared unbiased estimators for different number of subnetworks of three oscillators in a network of 12 oscillators. As expected, increasing the number of subnetworks increases the multivariate synchrony for both estimators.

C. Cognitive Control: A Study of Error-Related Negativity

In order to assess the synchronized activity among various regions in the brain, we compared the proposed measure against the S-estimator in a cognitive control-related error processing study from multichannel EEG recordings [61]. Multivariate synchrony is vital in neuroscience since cognitive tasks rely on the integration of multiple functional regions over the brain [62], [63]. In particular, we assessed the error-related negativity (ERN) which is an event-related potential (ERP) that reaches its maximal amplitude within 100 ms after response errors in simple reaction time tasks [64]. The ERN has been associated with increased synchronization in the theta band (4–8 Hz) among the central and frontal regions, particularly the medial prefrontal cortex (mPFC) and the lateral prefrontal cortex (lPFC) [65], when compared to central and parietal regions [66].

TABLE III
MULTIVARIATE SYNCHRONY (MEAN±ST.DEV.) FOR A NETWORK CONSISTING OF 12 OSCILLATORS FOR DIFFERENT NUMBER OF SUBNETWORKS COMPOSED OF THREE OSCILLATORS

Number of Subnetworks	HTS	S	HTS^2_{UB}	S^2_{UB}
1	0.531±0.009	0.252±0.009	0.278±0.010	0.156±0.006
2	0.613±0.015	0.348±0.008	0.373±0.018	0.263±0.006
3	0.735±0.031	0.506±0.010	0.538±0.018	0.398±0.010
4	0.757±0.012	0.594±0.013	0.571±0.025	0.492±0.012

EEG data was provided from a previously published study where subjects performed a speeded-response flanker task [67]. In this experiment subjects were required to correctly identify the target letter, located at the center of a five-letter string. By pressing one mouse button, subjects identified the target letter being congruent (e.g., MMMMM) or incongruent (e.g., MMNMM) with respect to the flanker letters. Each trial was 135 ms long, where during the first 35 ms prior to the onset of the target letter only the flanker letters (e.g., MM MM) were presented and then the five letters were kept on the screen during the remaining 100 ms. Inter-trial intervals ranged between 1 200 ms to 1 700 ms and a fixation cross was presented during that time. The experiment entailed a total of six blocks of 80 trial and the letters were changed between blocks.

EEG activity from error and correct responses was recorded by the ActiveTwo system (BioSemi, Amsterdam, The Netherlands). Epochs were 1200 ms long, with the beginning 200 ms belonging to the time prior to the response. All epochs were processed using the Current Source Density (CSD) Toolbox for volume conduction [68], after correction for eye movement artifacts and rejection of trials containing artifacts. Nineteen subjects whose error trials ranged from 20 to 61 (36.78 ± 13.72, mean $\pm$ st.dev.), were considered in this analysis and the same number of correct responses was chosen randomly. The sampling frequency of the EEG epochs was 512 Hz. Fig. 7 illustrates the locations of the 58 electrodes considered in this work.

We investigated topographical connectivity by computing the multivariate synchrony of error and correct responses separately at each electrode among it and its four nearest neighbors. For example, multivariate synchrony at electrode FCz will include electrodes FCz, Fz, FC2, Cz, and FC1. For each subject, HTS and S-estimator were computed as in (24) and (6), respectively, resulting in a multivariate synchrony time and frequency map. In order to consider the multivariate synchrony occurring during the peak of the ERN (50–75 ms) [69] and the onset of the ERN, we selected a time window of 25–75 ms. This is similar to our

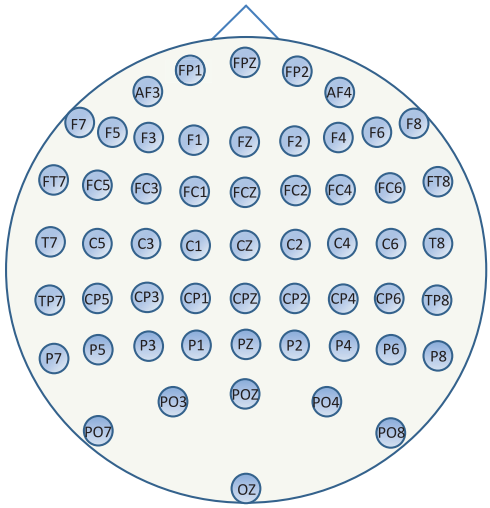

Fig. 7. Locations and names of electrodes.

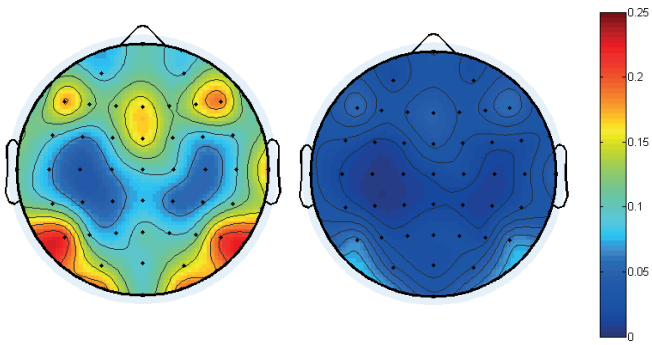

(a) (b)

Fig. 8. Topographical error-correct synchrony plots for (a) HTS, (b) S-Estimator.

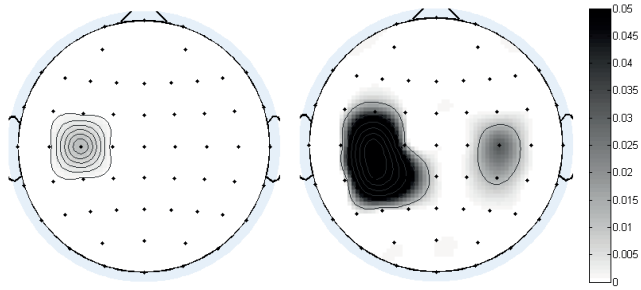

(a) (b)

Fig. 9. Topographical p-values of error vs. correct multivariate synchrony (a) HTS, (b) S-Estimator. (White refers to significant differences).

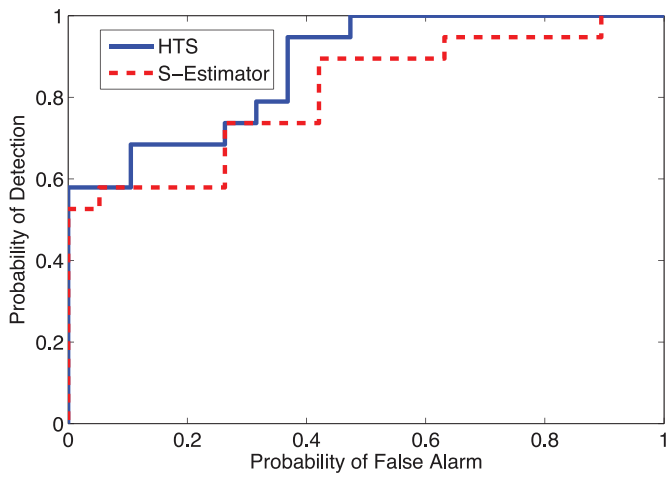

Fig. 10. ROC curves for HTS and S-Estimator. Probability of detection is based on the multivariate synchrony among FCz and its neighbors whereas the probability of false alarm is based on the multivariate synchrony around CPz.

previous work [20] as this time window showed the strongest differences between error and correct responses. In addition, we focus on the theta band since synchronization during the ERN interval has been shown to occur within this band [65]. Thus, time-frequency multivariate synchrony maps were averaged over the time interval [25 ms, 75 ms] and the theta band (4–8 Hz) for each electrode, resulting in a single multivariate synchrony value for each electrode to be used in the construction of topographical plots and statistical significance tests.

Fig. 8(a) and (b) illustrate the topological distribution of multivariate synchrony for error minus correct responses averaged over subjects estimated from HTS and S-estimator, respectively. HTS results in higher synchrony differences for error versus correct responses for the frontal and central electrodes when compared to the central-parietal electrodes, following previous hypotheses. We performed a Wilcoxon rank-sum test over all subjects (19) in order to compare the multivariate synchrony from error and correct responses obtained from both methods at each electrode. Fig. 9(a) and (b) show the topoplots of p-values for HTS and S-estimator, respectively. Both estimators result in significant differences ($p < 0.01$, Wilcoxon rank-sum test) in the central-frontal regions. However, the two methods differ slightly in the significant error-correct differences in the central-lateral regions. In particular, HTS detects significantly different synchrony in the right-central region with this significant difference nonexistent for the left-central region. Although in a lower degree, this is also observed for the S-estimator where the right frontal-central electrodes show significant differences between error and correct while the left frontal-central electrodes do not. This finding is in agreement with previous cognitive control studies that showed higher clustering and bivariate synchrony in the right-central region compared to the left-central region [70], [71]. This lateralization in synchrony is in agreement with findings in functional imaging studies on emotion regulation which have linked activity in the right hemisphere to cognitive control tasks [72].

In addition, a Receiver Operating Characteristic (ROC) curve was constructed in order to compare the performance of HTS and the S-estimator in the detection of multivariate synchrony during the ERN interval in the theta band. The probability of detection and false alarm were defined as the ratio at which the average multivariate synchrony over the ERN interval and theta band in electrodes FCz and CPz, respectively, exceeded a threshold. Fig. 10 shows the ROC curves for both estimators. The area under the curve (AUC) for each estimator was computed, resulting in $\mathrm{AUC}_{\mathrm{HTS}} = 0.8601$ and $\mathrm{AUC}_{S-\mathrm{estimator}} = 0.7936$. Thus, as observed, HTS exceeds S-estimator in the detection of multivariate synchronization in the frontal-central re-

gions during the ERN in the theta band indicating that HTS is more sensitive to detecting the difference in synchronization between the frontal-central region and the central-parietal region.

VII. Conclusion

In this work, we presented a novel time-frequency measure of multivariate phase synchrony based on a hyperdimensional coordinate system. This measure has been derived from both a hyperspherical coordinate system and from the Cartesian product of unit circles. The proposed measure has been shown to be advantageous over a widely used multivariate measure, the S-estimator, in estimating the global synchrony in simulated systems of coupled oscillators and in neurophysiological signals. In particular, it was shown that the proposed method is a direct measure of global synchrony which overcomes the drawbacks of multivariate synchrony methods based on the bivariate PLV. First, it was shown, from a simulation in Rössler oscillators, that the proposed measure provides information about the underlying structure of the network, otherwise misinterpreted from the S-estimator. Second, the proposed measure is computationally efficient since it does not require the computation of all pairwise synchrony values in a network nor the eigendecomposition of a connectivity matrix. In addition, this measure is effective in detecting multivariate synchrony in the frontal-central regions during the ERN. Furthermore, the proposed measure can be implemented using instantaneous phase estimates obtained from the Hilbert transform, the Wavelet transform and, with some limitations, the Hilbert-Huang transform in addition to the RID-Rihaczek distribution. Thus, the proposed measure of multivariate synchrony is a promising tool for the assessment of the global integration in dynamic complex networks.

Acknowledgment

The authors would like to thank Dr. Jason S. Moser from the Psychology Department at Michigan State University for providing the EEG data.

References

[1] C. Liu, D. R. Weaver, S. H. Strogatz, and S. M. Reppert, "Cellular construction of a circadian clock: Period determination in the suprachiasmatic nuclei," *Cell*, vol. 91, no. 6, pp. 855–860, 1997.

[2] F. Varela, J.-P. Lachaux, E. Rodriguez, and J. Martinerie, "The brainweb: Phase synchronization and large-scale integration," *Nature Rev. Neurosci.*, vol. 2, no. 4, pp. 229–239, 2001.

[3] J. Buck, "Synchronous rhythmic flashing of fireflies. II," *Quart. Rev. Biol.*, pp. 265–289, 1988.

[4] K. Wiesenfeld, P. Colet, and S. H. Strogatz, "Frequency locking in josephson arrays: Connection with the kuramoto model," *Phys. Rev. E*, vol. 57, no. 2, pp. 1563–1569, 1998.

[5] S. H. Strogatz, D. M. Abrams, A. McRobie, B. Eckhardt, and E. Ott, "Theoretical mechanics: Crowd synchrony on the millennium bridge," *Nature*, vol. 438, no. 7064, pp. 43–44, 2005.

[6] N. J. Fliege and J. Wintermantel, "Complex digital oscillators and fsk modulators," *IEEE Trans. Signal Process.*, vol. 40, no. 2, pp. 333–342, 1992.

[7] Y. Wang, F. Nunez, and F. J. Doyle, "Statistical analysis of the pulse-coupled synchronization strategy for wireless sensor networks," *IEEE Trans. Signal Process.*, vol. 61, no. 21, pp. 5193–5204, 2013.

[8] Y. Wang, F. Nunez, and F. J. Doyle, III, "Energy-efficient pulse-coupled synchronization strategy design for wireless sensor networks through reduced idle listening," *IEEE Trans. Signal Process.*, vol. 60, no. 10, pp. 5293–5306, 2012.

[9] Y. Wang and F. J. Doyle, "Optimal phase response functions for fast pulse-coupled synchronization in wireless sensor networks," *IEEE Trans. Signal Process.*, vol. 60, no. 10, pp. 5583–5588, 2012.

[10] M. Rosenblum, A. Pikovsky, J. Kurths, C. Schäfer, and P. A. Tass, "Phase synchronization: From theory to data analysis," in *Handbook of Biological Physics*. Amsterdam, The Netherlands: Elsevier Science B. V., 2001, vol. 4, pp. 279–321.

[11] A. Pikovsky, M. Rosenblum, and J. Kurths, *Synchronization: A Universal Concept in Nonlinear Systems*, ser. Cambridge Nonlinear Science Series. Cambridge, U.K.: Cambridge Univ. Press, 2001, vol. 12.

[12] S. Boccaletti, J. Kurths, G. Osipov, D. Valladares, and C. Zhou, "The synchronization of chaotic systems," *Phys. Rep.*, vol. 366, no. 1, pp. 1–101, 2002.

[13] M. Le Van Quyen, J. Foucher, J. Lachaux, E. Rodriguez, A. Lutz, J. Martinerie, and F. Varela, "Comparison of Hilbert transform and wavelet methods for the analysis of neuronal synchrony," *J. Neurosci. Methods*, vol. 111, no. 2, pp. 83–98, 2001.

[14] T. M. Rutkowski, D. P. Mandic, A. Cichocki, and A. W. Przybyszewski, "EMD approach to multichannel EEG data the amplitude and phase components clustering analysis," *J. Circuits, Syst., Comput.*, vol. 19, no. 01, pp. 215–229, 2010.

[15] A. Ahrabian and D. P. Mandic, "Estimation of phase synchrony using the synchrosqueezing transform," in *Proc. IEEE Int. Conf. Acoust., Speech, Signal Process. (ICASSP)*, 2014, pp. 759–763.

[16] A. Y. Mutlu and S. Aviyente, "Multivariate empirical mode decomposition for quantifying multivariate phase synchronization," *EURASIP J. Adv. Signal Process.*, vol. 2011, pp. 1–13, 2011.

[17] A. Omidvarnia, G. Azemi, P. B. Colditz, and B. Boashash, "A time-frequency based approach for generalized phase synchrony assessment in nonstationary multivariate signals," *Digit. Signal Process.*, vol. 23, no. 3, pp. 780–790, 2013.

[18] A. Ahrabian, C. C. Took, and D. P. Mandic, "Algorithmic trading using phase synchronization," *IEEE J. Sel. Topics Signal Process.*, vol. 6, no. 4, pp. 399–404, 2012.

[19] S. Aviyente and A. Mutlu, "A time-frequency-based approach to phase and phase synchrony estimation," *IEEE Trans. Signal Process.*, vol. 59, no. 7, pp. 3086–3098, 2011.

[20] S. Aviyente, E. Bernat, W. Evans, and S. Sponheim, "A phase synchrony measure for quantifying dynamic functional integration in the brain," *Human Brain Mapping*, vol. 32, no. 1, pp. 80–93, 2011.

[21] E. Pereda, R. Quiroga, and J. Bhattacharya, "Nonlinear multivariate analysis of neurophysiological signals," *Progr. Neurobiol.*, vol. 77, no. 1–2, pp. 1–37, 2005.

[22] R. Q. Quiroga, A. Kraskov, T. Kreuz, and P. Grassberger, "Performance of different synchronization measures in real data: A case study on electroencephalographic signals," *Phys. Rev. E*, vol. 65, no. 4, p. 041903, 2002.

[23] D. Cui, X. Liu, Y. Wan, and X. Li, "Estimation of genuine and random synchronization in multivariate neural series," *Neural Netw.*, vol. 23, no. 6, pp. 698–704, 2010.

[24] T. Koenig, D. Lehmann, N. Saito, T. Kuginuki, T. Kinoshita, and M. Koukkou, "Decreased functional connectivity of EEG theta-frequency activity in first-episode, neuroleptic-naíve patients with Schizophrenia: Preliminary results," *Schizophrenia Res.*, vol. 50, no. 1, pp. 55–60, 2001.

[25] M. Jalili, S. Lavoie, P. Deppen, R. Meuli, K. Q. Do, M. Cuénod, M. Hasler, O. De Feo, and M. G. Knyazeva, "Dysconnection topography in Schizophrenia revealed with state-space analysis of EEG," *PLoS One*, vol. 2, no. 10, p. e1059, 2007.

[26] M. Jalili, E. Barzegaran, and M. Knyazeva, "Synchronization of EEG: Bivariate and multivariate measures," *IEEE Trans. Neural Syst. Rehabil. Eng.*, vol. 22, no. 2, pp. 212–221, 2014.

[27] M. G. Knyazeva, M. Jalili, A. Brioschi, I. Bourquin, E. Fornari, M. Hasler, R. Meuli, P. Maeder, and J. Ghika, "Topography of EEG multivariate phase synchronization in early Alzheimer's disease," *Neurobiol. Aging*, vol. 31, no. 7, pp. 1132–1144, 2010.

[28] D. Rudrauf, A. Douiri, C. Kovach, J. Lachaux, D. Cosmelli, M. Chavez, C. Adam, B. Renault, J. Martinerie, and M. Le Van Quyen, "Frequency flows and the time-frequency dynamics of multivariate phase synchronization in brain signals," *Neuroimage*, vol. 31, no. 1, pp. 209–227, 2006.

[29] C. Allefeld and J. Kurths, "An approach to multivariate phase synchronization analysis and its application to event-related potentials," *Int. J. Bifurcation Chaos*, vol. 14, no. 2, pp. 417–426, 2004.

[30] M. J. Richardson, R. L. Garcia, T. D. Frank, M. Gergor, and K. L. Marsh, "Measuring group synchrony: A cluster-phase method for analyzing multivariate movement time-series," *Frontiers Physiol.*, vol. 3, 2012.

[31] C. Allefeld, M. Müller, and J. Kurths, "Eigenvalue decomposition as a generalized synchronization cluster analysis," *Int. J. Bifurcation Chaos*, vol. 17, pp. 3493–3497, 2007.

[32] A. S. Fine, D. P. Nicholls, and D. J. Mogul, "Assessing instantaneous synchrony of nonlinear nonstationary oscillators in the brain," *J. Neurosci. Methods*, vol. 186, no. 1, pp. 42–51, 2010.

[33] C. Allefeld and S. Bialonski, "Detecting synchronization clusters in multivariate time series via coarse-graining of Markov chains," *Phys. Rev. E*, vol. 76, no. 6, pp. 66207–66215, 2007.

[34] N. Saito, T. Kuginuki, T. Yagyu, T. Kinoshita, T. Koenig, R. D. Pascual-Marqui, K. Kochi, J. Wackermann, and D. Lehmann, "Global, regional, and local measures of complexity of multichannel electroencephalography in acute, neuroleptic-naive, first-break schizophrenics," *Biological Psychiatry*, vol. 43, no. 11, pp. 794–802, 1998.

[35] C. Stam and B. Van Dijk, "Synchronization likelihood: An unbiased measure of generalized synchronization in multivariate data sets," *Phys. D, Nonlinear Phenom.*, vol. 163, no. 3, pp. 236–251, 2002.

[36] J. Dauwels, F. Vialatte, T. Musha, and A. Cichocki, "A comparative study of synchrony measures for the early diagnosis of Alzheimer's disease based on EEG," *NeuroImage*, vol. 49, no. 1, pp. 668–693, 2010.

[37] C. Carmeli, M. G. Knyazeva, G. M. Innocenti, and O. De Feo, "Assessment of EEG synchronization based on state-space analysis," *Neuroimage*, vol. 25, no. 2, pp. 339–354, 2005.

[38] A. Y. Mutlu and S. Aviyente, "Hyperspherical phase synchrony for quantifying multivariate phase synchronization," in *Proc. IEEE Statist. Signal Process. Workshop (SSP)*, 2012, pp. 888–891.

[39] A. Y. Mutlu and S. Aviyente, "Hyperspherical phase synchrony measure for quantifying global synchronization in the brain," in *Proc. IEEE Int. Conf. Acoust., Speech, Signal Process. (ICASSP)*, 2013, pp. 1267–1271.

[40] J. P. Lachaux, A. Lutz, D. Rudrauf, D. Cosmelli, M. Le Van Quyen, J. Martinerie, and F. Varela, "Estimating the time-course of coherence between single-trial brain signals: An introduction to wavelet coherence," *Neurophysiologie Clinique/Clinic. Neurophysiol.*, vol. 32, no. 3, pp. 157–174, 2002.

[41] N. Rehman and D. P. Mandic, "Multivariate empirical mode decomposition," in *Proc. Roy. Soc. London A, Math., Phys. Eng. Sci.*, 2010, vol. 466, pp. 1291–1302.

[42] N. I. Fisher, *Statistical Analysis of Circular Data*. Cambridge, U.K.: Cambridge Univ. Press, 1995.

[43] J. M. Lee, *Riemannian Manifolds: An Introduction to Curvature*. New York, NY, USA: Springer Science & Business Media, 2006, vol. 176.

[44] J. Jost, *Riemannian Geometry and Geometric Analysis*. New York, NY, USA: Springer Science & Business Media, 2008.

[45] M. L. Oristaglio and B. R. Spies, *Three-Dimensional Electromagnetics*. Tulsa, OK, USA: SEG Books, 1999, no. 7.

[46] P. Renteln, *Manifolds, Tensors, and Forms: An Introduction for Mathematicians and Physicists*. Cambridge, U.K.: Cambridge Univ. Press, 2013.

[47] S. Mallat, *A Wavelet Tour of Signal Processing*. New York, NY, USA: Academic, 1999.

[48] D. Henderson, "Elementary functions: Algorithms and implementation," *Math. Comput. Educ.*, vol. 34, no. 1, p. 94, 2000.

[49] J. Demmel, I. Dumitriu, and O. Holtz, "Fast linear algebra is stable," *Numer. Math.*, vol. 108, no. 1, pp. 59–91, 2007.

[50] I. N. Bronštejn and K. A. Semendjaev, *Handbook of Mathematics*. New York, NY, USA: Springer, 2013.

[51] K. Mardia, *Statistics of Directional Data: Probability and Mathematical Statistics*. London, U.K.: Academic, 1972, p. 357.

[52] S. Aydore, D. Pantazis, and R. M. Leahy, "A note on the phase locking value and its properties," *Neuroimage*, vol. 74, pp. 231–244, 2013.

[53] M. Vinck, M. van Wingerden, T. Womelsdorf, P. Fries, and C. M. Pennartz, "The pairwise phase consistency: A bias-free measure of rhythmic neuronal synchronization," *Neuroimage*, vol. 51, no. 1, pp. 112–122, 2010.

[54] Y. Kuramoto, "Self-entrainment of a population of coupled non-linear oscillators," in *Proc. Int. Symp. Math. Problems Theoretic. Phys.*, 1975, pp. 420–422.

[55] S. H. Strogatz, "From Kuramoto to Crawford: Exploring the onset of synchronization in populations of coupled oscillators," *Phys. D, Nonlinear Phenom.*, vol. 143, no. 1, pp. 1–20, 2000.

[56] A. Takamatsu, T. Fujii, and I. Endo, "Time delay effect in a living coupled oscillator system with the plasmodium of physarum polycephalum," *Phys. Rev. Lett.*, vol. 85, no. 9, pp. 2026–2029, 2000.

[57] C. J. Stam, G. Nolte, and A. Daffertshofer, "Phase lag index: Assessment of functional connectivity from multi channel EEG and MEG with diminished bias from common sources," *Human Brain Mapping*, vol. 28, no. 11, pp. 1178–1193, 2007.

[58] S. H. Strogatz, "Exploring complex networks," *Nature*, vol. 410, no. 6825, pp. 268–276, 2001.

[59] B. Schelter, M. Winterhalder, R. Dahlhaus, J. Kurths, and J. Timmer, "Partial phase synchronization for multivariate synchronizing systems," *Phys. Rev. Lett.*, vol. 96, no. 20, p. 208103, 2006.

[60] B. Veeramani, K. Narayanan, A. Prasad, L. D. Iasemidis, A. S. Spanias, and K. Tsakalis, "Measuring the direction and the strength of coupling in nonlinear systems—A modeling approach in the state space," *IEEE Signal Process. Lett.*, vol. 11, no. 7, pp. 617–620, 2004.

[61] S. Baillet, J. C. Mosher, and R. M. Leahy, "Electromagnetic brain mapping," *IEEE Signal Process. Mag.*, vol. 18, no. 6, pp. 14–30, 2001.

[62] K. J. Friston, K. Stephan, and R. Frackowiak, "Transient phase-locking and dynamic correlations: Are they the same thing?," *Human Brain Mapping*, vol. 5, no. 1, pp. 48–57, 1997.

[63] R. Bashirullah, J. G. Harris, and J. A. Fortes, "Technology and signal processing for brain-machine interfaces," *IEEE Signal Process. Mag.*, vol. 25, no. 1, pp. 29–40, 2008.

[64] J. S. Moser, T. P. Moran, H. S. Schroder, M. B. Donnellan, and N. Yeung, "On the relationship between anxiety and error monitoring: A meta-analysis and conceptual framework," *Frontiers Human Neurosci.*, vol. 7, 2013, doi: 10.3389/fnhum.2013.00466.

[65] J. Cavanagh, M. Cohen, and J. Allen, "Prelude to and resolution of an error: EEG phase synchrony reveals cognitive control dynamics during action monitoring," *J. Neurosci.*, vol. 29, no. 1, pp. 98–105, 2009.

[66] M. Cohen, "Error-related medial frontal theta activity predicts cingulate-related structural connectivity," *Neuroimage*, vol. 55, no. 3, pp. 1373–1383, 2011.

[67] T. P. Moran, E. M. Bernat, S. Aviyente, H. S. Schroder, and J. S. Moser, "Sending mixed signals: Worry is associated with enhanced initial error processing but reduced call for subsequent cognitive control," *Social Cognit. Affect. Neurosci.*, p. nsv046, 2015.

[68] J. Kayser and C. Tenke, "Principal components analysis of Laplacian waveforms as a generic method for identifying ERP generator patterns: I. Evaluation with auditory oddball tasks," *Clinic. Neurophysiol.*, vol. 117, no. 2, pp. 348–368, 2006.

[69] J. R. Hall, E. M. Bernat, and C. J. Patrick, "Externalizing psychopathology and the error-related negativity," *Psychol. Sci.*, vol. 18, no. 4, pp. 326–333, 2007.

[70] M. Bolanos, E. M. Bernat, B. He, and S. Aviyente, "A weighted small world network measure for assessing functional connectivity," *J. Neurosci. Methods*, vol. 212, no. 1, pp. 133–142, 2013.

[71] A. Ozdemir, M. Bolanos, E. M. Bernat, and S. Aviyente, "Hierarchical spectral consensus clustering for group analysis of functional brain networks," *IEEE Trans. Biomed. Eng.*, vol. 62, no. 9, pp. 2158–2169, 2015.

[72] K. N. Ochsner, J. A. Silvers, and J. T. Buhle, "Functional imaging studies of emotion regulation: A synthetic review and evolving model of the cognitive control of emotion," *Ann. New York Acad. Sci.*, vol. 1251, no. 1, pp. E1–E24, 2012.

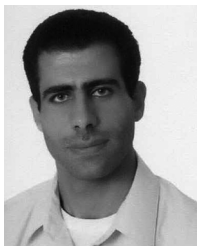

Mahmood Al-Khassaweneh (S'04–SM'13) was born in Irbid, Jordan, on June 11, 1977. He received the B.S. degree in electrical engineering from Jordan University of Science and Technology, Irbid, Jordan, in 2000, and the M.S. and the Ph.D. degrees in electrical engineering from Michigan State University, East Lansing, MI, USA, in 2003 and 2007, respectively.

Since Fall 2007, he has been working with the Department of Computer Engineering, Hijjawi Faculty for Engineering Technology, Yarmouk University, Irbid, Jordan. He has been working as a Visiting Associate Professor in the Electrical and Computer Engineering Department at Michigan State University, East Lansing, MI, USA, since Fall 2014. His research interests include Image Processing, Computer Vision, Medical Imaging, Data Security and applying signal processing methods to the brain signals.

Dr. Al-Khassaweneh is a member of Jordanian Engineers Association.

Marisel Villafañe-Delgado (S'08) received the B.S. degree in electronics engineering technology from the University of Puerto Rico, Bayamón, Puerto Rico, in 2008, the B.S. degree in electrical engineering from the University of Puerto Rico, Mayagüez, Puerto Rico, in 2011 and the M.S. degree in electrical engineering from the University of Maryland, College Park, MD, USA, in 2013. She is currently working towards the Ph.D. degree in electrical engineering at Michigan State University, East Lansing, MI.

She has worked as research intern at the National Institute of Standards and Technology (2007), the University of Maryland (2009) and the Massachusetts Institute of Technology Lincoln Laboratory (2010 and 2011).

Ms. Villafañe-Delgado was awarded the National Science Foundation Graduate Research Fellowship in 2011, the George Simon Ohm award to the best student in Electrical Engineering from the University of Puerto Rico at Mayagüez in 2011 and the medal to the highest G.P.A. in the 2008 class of Electronics Engineering Technology from the University of Puerto Rico at Bayamón.

Ali Yener Mutlu (M'13) received the B.S. degree in electrical and electronics engineering from Boğaziçi University, Istanbul, Turkey in 2008 and the Ph.D. degree in electrical engineering from Michigan State University, East Lansing, MI, USA in 2012.

He worked as a senior R&D Strategist at Genband-Netas where he brought innovative ideas, designed project architectures, prepared project proposals for Horizon 2020 and EUREKA (Celtic Plus and ITEA clusters) funding programs. He acted as the project manager and coordinator of the first European Union project of Genband-Netas. He is currently an Assistant Professor at the Department of Computer Engineering, Izmir University of Economics, Izmir, Turkey. He has been working on the theory and applications of statistical signal processing algorithms, in particular using non-stationary signal analysis and time-frequency distributions. His research is focused on the study of functional networks in the human brain based on electroencephalogram (EEG) data for a better understanding of brain diseases such as epilepsy, schizophrenia and Alzheimers disease.

Dr. Mutlu received the "College of Engineering Outstanding Graduate Research Award" at Michigan State University.

Selin Aviyente (M'97) received the B.S. degree with high honors in electrical and electronics engineering from Boğaziçi University, Istanbul, Turkey in 1997, the M.S. and Ph.D. degrees, both in electrical engineering: systems, from the University of Michigan, Ann Arbor, MI, USA, in 1999 and 2002, respectively.

Currently, she is an Associate Professor in the Department of Electrical and Computer Engineering at Michigan State University, East Lansing, MI, USA. Her research focuses on statistical signal processing, in particular non-stationary signal analysis, with applications to biological signals. Her most recent work focuses on the study of the dynamic functional networks in the brain using EEG and fMRI.

Dr. Aviyente is the recipient of the 2005 Withrow Teaching Excellence Award and the 2008 NSF CAREER Award. She was the special session organizer for IEEE Statistical Signal Processing (SSP) Workshop in 2012 and the technical area chair for Biomedical Image and Signal Processing for Asilomar Conference in 2014. She is currently a Senior Area Editor for IEEE TRANSACTIONS ON SIGNAL PROCESSING.